Rigid Oxazole Acinetobactin Analog Blocks Siderophore Cycling in *Acinetobacter baumannii*

Supporting Information

Tabbetha J. Bohac[1], Justin A. Shapiro[1] and Timothy A. Wencewicz*

[1]These authors contributed equally to this work.

Department of Chemistry, Washington University in St. Louis, One Brookings Drive, St. Louis, MO, 63130, USA

Table of Contents

*Correspondence to TAW: Email: wencewicz@wustl.edu; Ph: 314-935-7247; Fax: 314-935-4481; ORCID: 0000-0002-5839-6672

I. Materials and Methods

Strains, Materials, and Instrumentation

Growth studies were conducted using *A. baumannii* ATCC 19606TT and derivatives t6 (bauA::EZ::TN<R6Kcori/KAN-2>), t7 (bauD::EZ::TN<R6Kcori/KAN-2>), and s1 (basD::aph) provided by Dr. Luis Actis. Precultures and 96-well plate *A. baumannii* growth assays were performed in filter-sterilized M9 minimal media. Samples for LC-MS were prepared in 0.45 μM PTFE mini-UniPrep vials from Agilent. All preparatory HPLC was performed using a Beckman Coulter SYSTEM GOLD 127P solvent module and 168 detector with a Phenomenex Luna 10u C18(2) 100A column, 250 × 21.20 mm, 10 μm with guard column. Prep HPLC was performed with a mobile phase of 5 mM ammonium acetate in (A) water and (B) acetonitrile, and data were processed using 32 Karat software, version 7.0. All LC-MS was performed on an Agilent 6130 quadrupole LC-MS with G1313 autosampler, G1315 diode array detector, and 1200 series solvent module. A Phenomenex Gemini C18 column, 50 × 2 mm, 5 μm with guard column was used for all LC-MS separations. LC-MS mobile phases were 0.1% formic acid in (A) water and (B) acetonitrile, and data were processed using G2710 ChemStation software. NMR was performed on a Varian Unity Inova-600 MHz instrument with a cold probe. Bacterial growth studies were performed using polystyrene 96-well plates with polystyrene lids. OD600 measurements were taken on a Molecular Devices SpectraMax Plus 384 plate reader.

Acinetobactin Isolation

Natural acintobactin was isolated and purified from *A. baumannii* cultures as previously reported.[1] Briefly, liter cultures of *A. baumannii* ATCC 17978 were grown overnight in M9 minimal media. The cultures were centrifuged down and the supernatant was adjusted to pH 6. XAD-7HP resin was added and the supernatant was shaken. The resin was washed with methanol. The methanol extract was concentrated and preparatory HPLC purified to yield pure acinetobactin.

Compound Synthesis

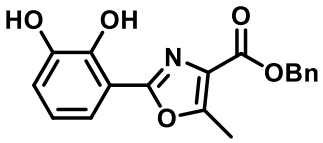

Benzyl 2-(2,3-dihydroxyphenyl)-5-methyloxazole-4-carboxylate (8). The synthesis of **8** was adapted from a previously reported, one-pot synthesis of oxazoles.[2] To a clean, dry round bottom flask equipped with a stirbar and argon inlet was added *L*-throenine benzyl ester oxalate (1.0 g, 3.34 mmol), potassium carbonate (0.92 g, 6.68 mmol), and *N*,*N*'-dimethylacetamide (8.3 mL) (Note: a white, cloudy solution was formed). To the resultant mixture was added 2,3-dihydroxybenzaldehyde (0.46 g, 3.34 mmol) [solid, in one portion], which resulted in the formation of a bright yellow solution which stirred at room temperature, under argon, for 12 hrs. After 12 hrs, the reaction was cooled to 0°C, and bromotrichloromethane (0.99 mL, 10.02 mmol) and 1,8-diazabicyclo[5.4.0]undec-7-ene (1.50 mL, 10.02 mmol) were added. The resulting deep orange solution was stirred at 0°C for 2 hrs, at which point the reaction was removed from the ice bath and warmed to rt. The mixture stirred at rt for an additional 10 hrs [monitored by LC-MS]. The reaction was diluted with DD-H_2O (3x original volume) and extracted with MTBE (3 x 15 mL) and EtOAc (3 x 15 mL). The organic layers were combined, washed with brine, and dried over Na_2SO_4. The product was concentrated by rotary evaporation to yield a dark orange sticky solid (0.92 g, 85% crude yield). The crude product was then purified as needed by prep HPLC (gradient of 0% B to 95% B for 17 min then hold at 100% B for 8 minutes) to provide the title compound as a pale yellow oil (5 mg per injection, yielded 3.5 mg of pure compound). ^{1}H NMR (600 MHz, Chloroform-*d*) δ 7.46 (d, *J* = 7.1 Hz, 2H), 7.43 – 7.33 (m, 4H), 7.31 (d, *J* = 8.0 Hz, 1H), 7.03 (d, *J* = 7.9 Hz, 1H), 6.86 (t, *J* = 7.9 Hz, 1H), 5.38 (s, 2H), 2.70 (s, 3H). ^{13}C NMR (151 MHz, Chloroform-*d*) δ 161.5, 159.5, 155.4, 145.3, 144.7, 135.7, 128.8, 128.6, 128.4, 127.0, 120.0, 117.6, 116.9, 110.2, 66.8, 12.3. LC-MS cald for $C_{18}H_{16}NO_5$ $(M + H)^+$ 326.1028; found 326.1.

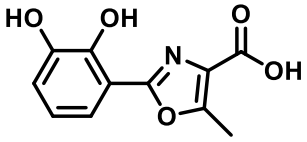

2-(2,3-dihydroxyphenyl)-5-methyloxazole-4-carboxylic acid (9). To a solution of oxazole **8** (20 mg, 0.06 mmol) in MeOH (2 mL) was added 10% P/C (2 mg) at rt. The vial was purged with H_2 and allowed to stir under H_2 atm (1 atm) for 1 hr [monitored by LC-MS]. Once complete, as judged by LC-MS, the solid catalyst was removed via syringe filtration, and the solution was concentrated under reduced pressure to provide pure carboxylic acid **9** as a clear colorless oil (99% yield). ^{1}H NMR (600 MHz, Methanol-d_4) δ 7.33 (d, J = 7.9 Hz, 1H), 6.94 (d, J = 7.9 Hz, 1H), 6.83 (t, J = 7.9 Hz, 1H), 2.72 (s, 3H). ^{13}C NMR (151 MHz, Methanol-d_4) δ 164.8, 160.8, 156.7, 147.2, 146.8, 128.5, 120.8, 119.4, 117.6, 111.7, 12.0. LC-MS cald for $C_{11}H_{10}NO_5$ $(M + H)^+$ 236.0559; found 236.1.

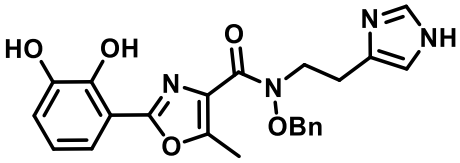

***N*-(2-(1*H*-imidazol-4-yl)ethyl)-*N*-(benzyloxy)-2-(2,3-dihydroxyphenyl)-5-methyloxazole-4-carboxamide (11).** To a clean, dry round bottom flask equipped with a stirbar and argon inlet was added carboxylic acid **9** (60 mg, 0.25 mmol), DMF (8 mL), and hydroxyhistamine **7** (82 mg, 0.38 mmol). To the stirring solution was added EDC (198 mg, 1.28 mmol) and HOBt (172 mg, 1.28 mmol), and Et_3N was added to the reaction dropwise until a pH of ~9 was obtained. The reaction stirred under argon for 12 hrs (monitored by LC-MS), at which point the reaction mixture was concentrated by rotary evaporation and purified by prep HPLC (gradient of 0% B to 95% B in 17 minutes, 95% B to 100% B in 2 minutes, hold 100% B for 8 minutes) to yield title compound **11** as a pale yellow oil (64 mg, 58% yield). ^{1}H NMR (600 MHz, DMSO-d_6) δ 7.49 (s, 1H), 7.38 – 7.26 (m, 5H), 7.20 (dd, J = 7.9, 1.6 Hz, 1H), 6.92 (d, J = 7.8 Hz, 1H), 6.79 (s, 1H), 6.75 (t, J = 7.8 Hz, 1H), 4.95 (s, 2H), 4.06 (t, J = 7.2 Hz, 2H), 2.87 (t, J = 7.2 Hz, 2H), 2.42 (s, 3H). ^{13}C NMR (151 MHz, DMSO-d_6) δ 172.0, 161.4, 157.9, 146.1, 145.1, 134.8, 129.3, 129.1, 128.6, 128.3, 119.6, 118.2, 116.5, 111.1, 75.6, 25.0, 21.1, 11.4. HRMS cald for $C_{23}H_{23}N_4O_5$ $(M + H)^+$ 435.1663; found 435.1669

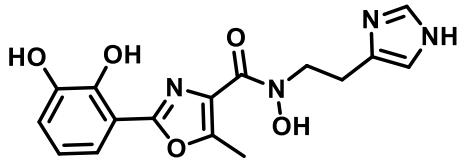

***N*-(2-(1*H*-imidazol-4-yl)ethyl)-2-(2,3-dihydroxyphenyl)-*N*-hydroxy-5-methyloxazole-4-carboxamide (3).** *O*-benzyl-oxidized-pre-acinetobactin **11** (12 mg, 0.05 mmol) was stirred in MeOH with ~1/10 mass equivalent of 10% Pd/C under H_2 atmosphere (1 atm). Upon confirmation of reaction completion by LC-MS (~1 hr), the solid catalyst was removed through syringe filtration and the solution was concentrated by rotary evaporation to provide oxidized preacinetobactin **3** as a colorless oil. ^{1}H NMR (600 MHz, DMSO-d_6) δ 7.54 (s, 1H), 7.23 (dd, J = 7.9, 1.6 Hz, 1H), 6.95 – 6.92 (m, 1H), 6.86 (s, 1H), 6.80 (t, J = 7.9 Hz, 1H), 3.93 (s, br, 2H), 2.88 (t, J = 7.3 Hz, 2H), 2.50 (s, 3H, under DMSO residual solvent peak). ^{13}C NMR (151 MHz, DMSO-d_6) δ 157.8, 151.4, 146.2, 145.3, 134.8, 128.0, 119.5, 118.2, 116.1, 110.7, 48.6, 11.4.HRMS cald for $C_{16}H_{17}N_4O_5$ $(M + H)^+$ 345.1199; found 345.1193.

Biological Studies

M9 minimal media was prepared for all experiments as previously described.[1]

For biological assessment of acinetobactin **2** and oxidized pre-acinetobactin **3** under iron-restrictive conditions, stock solutions of 800 μM **2** and **3** were prepared in M9 minimal media and filter sterilized. A 96-well plate was filled with 50 μL of M9 minimal media per well. Into the first column, 50 μL of either acinetobactin stock or oxidized pre-acinetobactin stock was added, and columns were serially diluted down to 1.56 μM. An inoculum was made by adding 200 μL of 0.5 McFarland standard (*A. baumannii* ATCC 19606TT s1) to 29.8 mL of M9 minimal media supplemented with 250 μM 2,2'-dipyridyl. Inoculum (50 μL) was added to each well for a final concentration of 125 μM 2,2'-dipyridyl and a serial dilution of 200-0.78 μM acinetobactin and oxidized pre-acinetobactin. Growth promotion or inhibition was determined as compared to a control with 125 μM 2,2'-dipyridyl, 0 μM acinetobactin and 0 μM oxidized pre-acinetobactin. All experiments were performed in triplicate. For confirmation of biological activity of re-purified compound, procedure was reproduced but with 200 μM 2,2'-dipyridyl inoculum for a final concentration of 100 μM 2,2'-dipyridyl.

For biological assessment of competition between acinetobactin **2** and oxidized pre-acinetobactin **3**, a stock solution of 800 μM **3** was prepared in M9 minimal media and filter sterilized. A 96-well plate was filled with 50 μL of M9 minimal media per well. Into the first column, 50 μL of oxidized pre-acinetobactin stock was added, and columns were serially diluted down to 1.56 μM. An inoculum was made by adding 200 μL of 0.5 McFarland (*A. baumannii* ATCC 19606TT s1) to 29.8 mL of M9 minimal media supplemented with 200 μM 2,2'-dipyridyl and 20 μM acinetobactin. Inoculum (50 μL) was added to each well for a final concentration of 100 μM 2,2'-dipyridyl, 10 μM acinetobactin, and a serial dilution of 200-0.78 μM oxidized pre-acinetobactin. Growth promotion or inhibition was determined as compared to a control with 100 μM 2,2'-dipyridyl, 10 μM acinetobactin, and 0 μM oxidized pre-acinetobactin. All experiments were performed in triplicate.

For the biological evaluation of the Fe^{3+}-complex of oxidized pre-acinetobactin, 200 μM stocks of acinetobactin-Fe^{3+} and oxidized pre-acinetobactin-Fe^{3+} were prepared in M9 minimal media and filter sterilized. A 96-well plate was filled with 50 μL of M9 minimal media per well. Into the first column, 50 μL of either acinetobactin-Fe^{3+} stock or oxidized pre-acinetobactin-Fe^{3+} stock was added, and columns were serially diluted down to 0.39 μM. An inoculum was made by

adding 200 μL of 0.5 McFarland standard (*A. baumannii* ATCC 19606TT s1) to 29.8 mL of M9 minimal media supplemented with 300 μM 2,2'-dipyridyl. Inoculum (50 μL) was added to each well for a final concentration of 150 μM 2,2'-dipyridyl and a serial dilution of 50-0.19 μM acinetobactin and oxidized pre-acinetobactin. Growth promotion was determined as compared to a control with 125 μM 2,2'-dipyridyl, 0 μM acinetobactin-Fe^{3+} and 0 μM oxidized pre-acinetobactin-Fe^{3+}. All experiments were performed in triplicate.

For MIC evaluation of oxidized pre-acinetobactin, stock solutions of 800 μM oxidized pre-acinetobactin and ciprofloxacin were prepared in M9 minimal media and filter sterilized. Eight 96-well plates were filled with 50 μL of M9 minimal media per well. For the first column of each plate, 50 μL of either oxidized pre-acinetobactin stock or ciprofloxacin stock was added, and columns were serially diluted down to 1.56 μM. Seven separate inocula were prepared by diluting 200 μL of appropriate 0.5 McFarland standard (*E. coli* ATCC 25922, *A. baumannii* ATCC 19606TT, *A. baumannii* ATCC 19606T t6, *A. baumannii* ATCC 19606T t7, or *A. baumannii* ATCC 19606T s1) in either plain M9 minimal media (all bacterial strains) or M9 minimal media supplemented with 20 μM $Fe(acac)_3$ (just *A. baumannii* ATCC 19606T and *A. baumannii* ATCC 19606T s1). Inocula (50 μL) were added to each well of separate plates for a final concentration of either 0 μM or 10 μM Fe^{3+} and a serial dilution of 200-0.78 uM oxidized pre-acinetobactin and ciprofloxacin. Growth was measured by endpoint OD_{600}. All experiments were performed in triplicate.

Determination of K_{Fe}

Stock solutions of 100 μM pre-acinetobactin **1**, acinetobactin **2**, and oxidized pre-acinetobactin **3** were prepared in 10 mM HEPES buffer and a UV-Vis scan was recorded. Next 120 μM EDTA was added and absorbance at 500 nm was measured over 800 minutes. Iron-binding affinity (K_{Fe}) was determined using the following calculations.

(1) $K_L = \frac{[FeL_2]}{[Fe^{3+}][L]^2}$ for the following equilibrium; $[Fe^{3+}] + 2[L] \rightleftharpoons [FeL_2]$

(2) $K_{FeEDTA} = \frac{[FeEDTA]}{[Fe^{3+}]\,[EDTA]}$ for the following equilibrium; $[Fe^{3+}] + [EDTA] \rightleftharpoons [FeEDTA]$

(3) $K_{Exchange} = \frac{K_L}{K_{FeEDTA}}$ for the following equilibrium; $[FeEDTA] + 2[L] \rightleftharpoons [FeL_2] + [EDTA]$

(4) $K_{Exchange} = \frac{[FeL_2][EDTA]}{[FeEDTA][L]^2}$

(5) $\Delta = \frac{Abs_{FeL_2} - Abs_{FeL+EDTA}}{\varepsilon_L}$

(6) $K_L = K_{FeEDTA} \times \frac{[FeL_2][EDTA]}{[FeEDTA][L]^2}$

(7) $[FeL_2] = \frac{Abs_{FeL_2}}{\varepsilon_L}$

(8) $[EDTA] = [EDTA]_T - \Delta$ where $[EDTA]_T$ = total EDTA added

(9) $[FeEDTA] = \Delta$

(10) $[L] = 2\Delta$

(11) K_{Fe} = apparent K_L

Fluorescence Quenching Titration

A solution of 570 μM oxidized pre-acinetobactin **3** in methanol was prepared and a fluorescence emission spectra was recorded ($\lambda_{excitation}$ = 330 nm). To determine stoichiometry of the complex between **3** and iron (III), $Fe(acac)_3$ was added 0.0438 equivalents at a time (1 μL of 10 μM $Fe(acac)_3$ added by Hamilton syringe) and emission spectra were recorded at 380 nm after each addition. Peak fluorescence (Abs_{380nm}) was plotted against iron (III) equivalents.

Computational Studies

All calculations were performed using Spartan '16. Oxidized pre-acinetobactin **3** and pre-acinetobactin **1** were modeled in Spartan. The lowest energy conformations were obtained using the minimize energy function. The 3'-4'-9-8 dihedral (see **Supplementary Table 1** for atom numbers) was constrained in both molecules as the energy profile was created investigating the rotation around the oxazole-carbonyl bond. The energy profile was run at ground state in the gas state with molecular mechanics MMFF. The energy was calculated in kJ/mol as the heterocycle-carbonyl bond rotated 360 degrees over 25 steps. The energy was plotted as against the 25 conformations.

II. Supplemental Figures

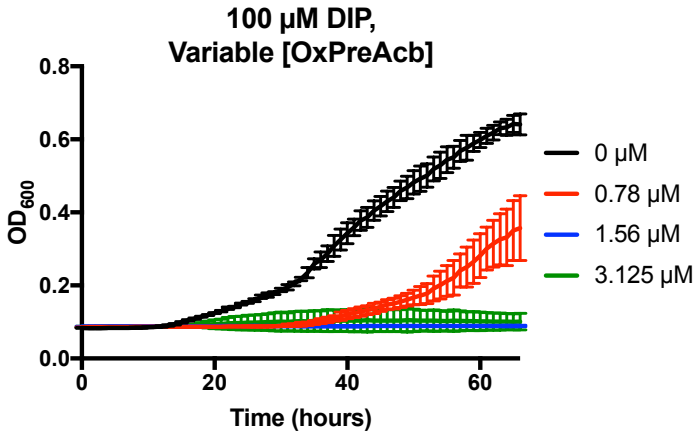

Supplementary Figure 1. Oxidized pre-acinetobactin (3) is a potent inhibitor of *Acinetobacter baumannii* ATCC 19606T growth in iron (III) controlled M9 minimal media. By reviewer request, the target compound was isolated to a greater degree of purity to ensure that extra signals from the NMR were not responsible for biological activity. Re-purified compound was then tested under new conditions to give an MIC_{90} reading. Compound **3** totally inhibited growth at 1.56 µM under these conditions. NMR and LC-MS data of re-purified compound can be found on supplementary page 26.

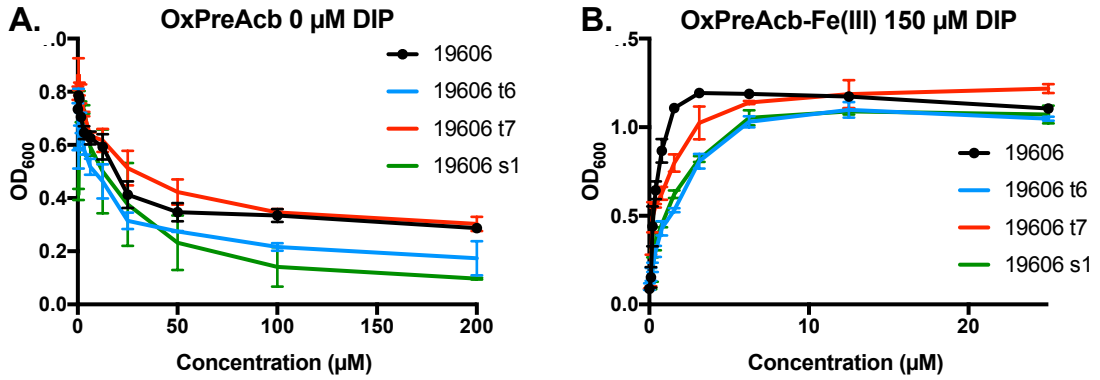

Concentration OxPreAcb (µM)	p-value (t6)	p-value (t7)	p-value (s1)
200	0.4929*	0.4452	0.0001***
100	0.002**	0.4935	0.0127*
50	0.0213*	0.0871*	0.1401
25	0.0450*	0.1042	0.7185
12.5	0.0474*	0.5530	0.3827
6.25	0.0084**	0.6228	0.2429
3.125	0.0252*	0.0095**	0.0068**
1.56	0.4204	0.0211*	0.4948
0.78	0.0053**	0.0941	0.2769
0.39	0.2244	0.0837	0.0001***
0	0.1018	0.0006***	0.2460

Concentration OxPreAcb-Fe(III) (µM)	p-value (t6)	p-value (t7)	p-value (s1)
25	0.0015**	0.0017**	0.3074
12.5	0.0495*	0.7924	0.004**
6.25	0.0016**	0.0112*	0.0072**
3.125	0.0001***	0.0363*	0.0001***
1.56	0.0001***	0.0005***	0.001**
0.78	0.0006***	0.0052**	0.0005***
0.39	0.0006***	0.0432*	0.0023**
0.195	0.0256*	0.5659	0.0033**
0.98	0.7008	0.5602	0.1355
0	0.2917	0.6997	0.1963

All p-values are relative to the wild type strain at equal concentration of added molecule.
* indicates a difference that is statistically significant.
** indicates a difference that is very statistically significant.
*** indicates a difference that is extremely statistically significant.

Supplementary Figure 2. OxPreAcb (3) promotes the growth of *A. baumannii* when complexed with iron (III). Endpoint OD_{600} measurements taken of bacterial growth of wild-type and mutants of *A. baumannii* ATCC 19606T in M9 minimal media. (A.) Media supplemented with gradient concentrations of oxidized pre-acinetobactin (**3**). Media contains 0 µM 2,2'-Dipyridyl. Measurements taken at 42 hours. (B.) Media supplemented with gradient concentrations of oxidized pre-acinetobactin (**3**) Fe(III)-Complex. Media contains 150 µM 2,2'-Dipyridyl. Measurements taken at 48 hours. Error bars represent standard deviations for three independent trials. All p-values and statistical significance are provided below in table format.

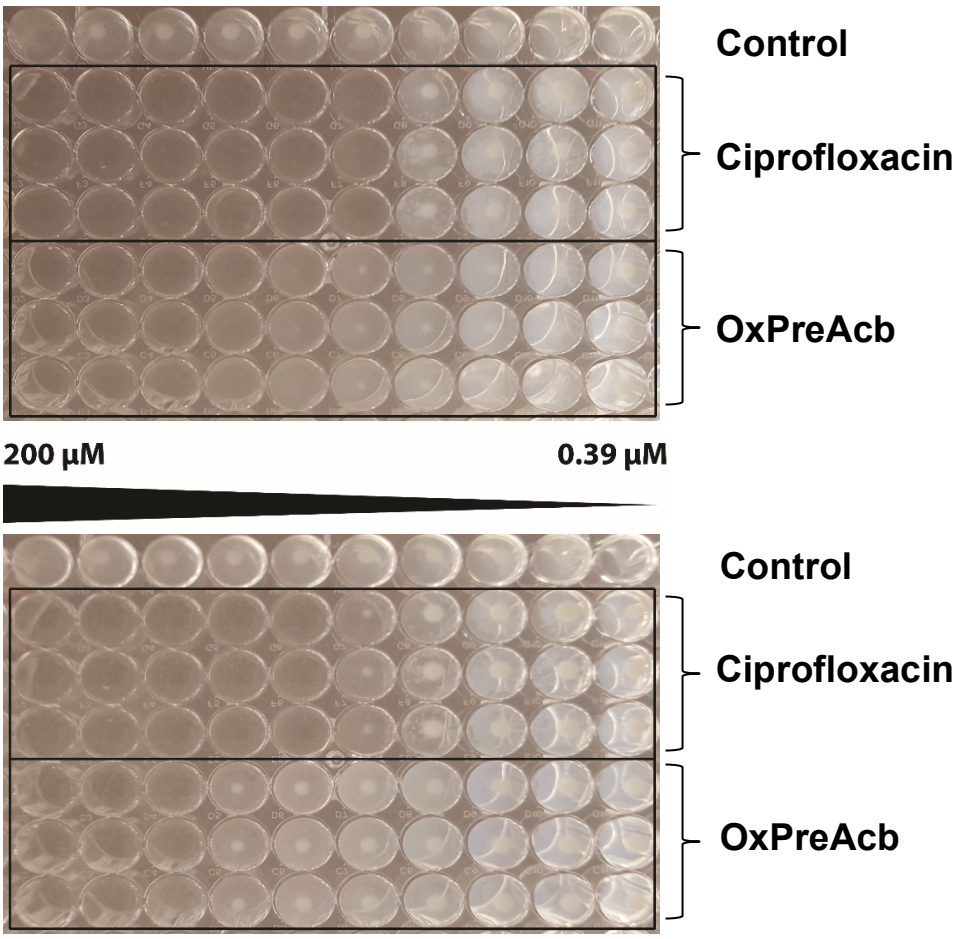

Supplementary Figure 3. The antibiotic effect of oxidized pre-acinetobactin (3) is bacteriostatic. Images of 96 well microplates at 42 hours (top) and 72 hours (bottom) showing dose dependent and bacteriostatic antibiotic effect of serially diluted oxidized pre-acinetobactin (**3**) against *A. baumannii* ATCC 19606T with a ciprofloxacin control. Wells in control rows contain no ciprofloxacin and no oxidized pre-acinetobactin. Growth curve analysis and regrowth studies of cells treated with OxPreAcb suggest no loss of viable *A. baumannii* cells upon treatment with OxPreAcb.

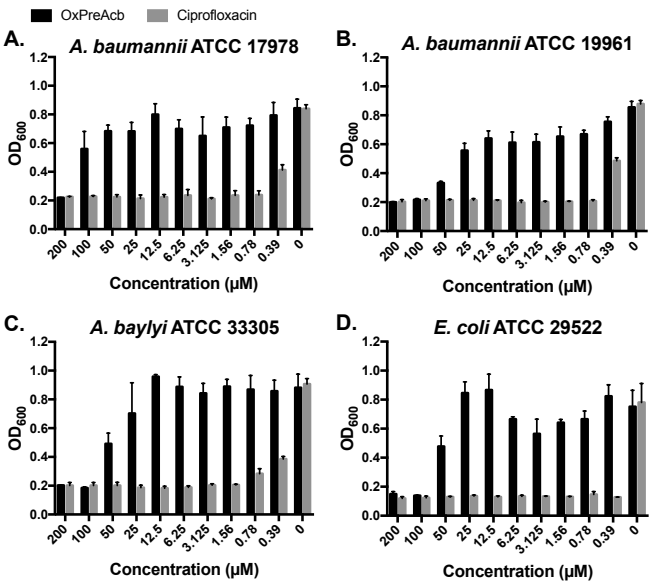

Supplementary Figure 4. Oxidized pre-acinetobactin (3) is bacteriostatic towards multiple strains of pathogenic *A. baumannii*, as well as environmental *Acinetobacter* and pathogenic *E. coli*. Endpoint OD_{600} measurements taken of bacterial growth in M9 minimal media supplemented with gradient concentrations of either oxidized pre-acinetobactin (**3**) or ciprofloxacin. (A.) *Acinetobacter baumannii* ATCC 17978. (B.) *Acinetobacter baumannii* ATCC 19961. (C.) *Acinetobacter baylyi* ATCC 33305. (D.) *Escherichia coli* ATCC 29522.

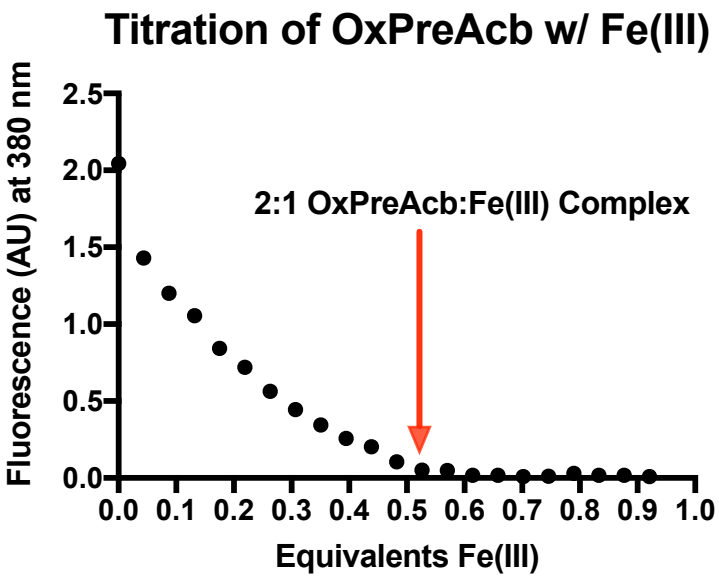

Supplementary Figure 5. Oxidized pre-acinetobactin (3) forms a stable 2:1 complex with iron (III). Graph shows the peak absorbance at 380 nm of emission spectra (λ_{ex} = 330 nm) of **3** (570 μM) with increasing quantities of $Fe(acac)_3$.

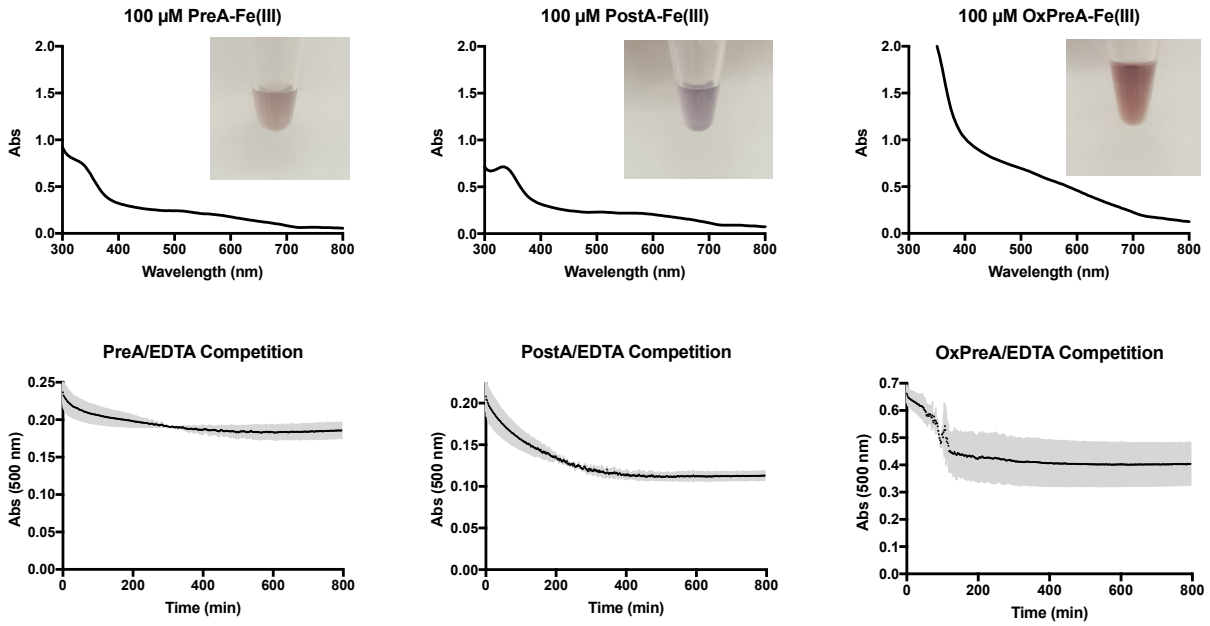

Supplementary Figure 6. Pre-acinetobactin, acinetobactin, and oxidized pre-acinetobactin all form colored, high-affinity complexes with iron(III). (A.) UV-Vis spectra of 100 µM pre-acinetobactin (**1**) complexed with iron (III) in 10 µM HEPES buffer. (B.) UV-Vis spectra of 100 µM oxidized pre-acinetobactin (**3**) complexed with iron (III) in 10 µM HEPES buffer. (C.) Kinetic single-wavelength (500 nm) scan of 100 µM pre-acinetobactin (**1**) complexed with iron (III) in HEPES supplemented with 120 µM EDTA. Black line represents average of two independent measurements and grey area represents standard deviation. Log(K_{Fe}) calculations provided in Equations 1–11. (D.) Kinetic single-wavelength (500 nm) scan of 100 µM oxidized pre-acinetobactin (**3**) complexed with iron (III) in HEPES supplemented with 120 µM EDTA. Black line represents average of two indpendent measurements and grey area represents standard deviation. Log(K_{Fe}) calculations provided in Equations 1–11. The apparent K_{Fe} values for the 2:1 PreAcb, Acb, and OxPreAcb iron(III) complexes were 27.4 ± 0.2, 26.2 ± 0.1, and 26.5 ± 0.3, respectively.

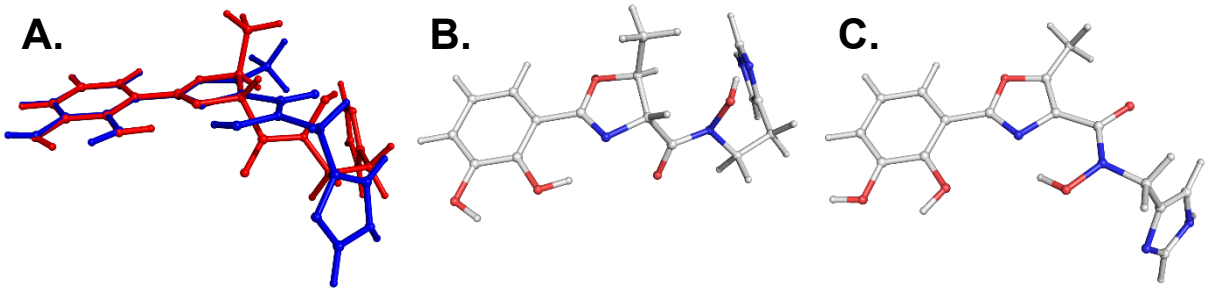

Supplementary Figure 7. Oxidized pre-acinetobactin is more rigid than pre-acinetobactin. Gas phase minimum energy calculation structures of (A.) pre-acinetobactin (red) overlaid with oxidized pre-acinetobactin (blue), (B.) pre-acinetobactin, and (C.) oxidized pre-acinetobactin. Pre-acinetobactin forms a stable intramolecular H-bond between the C2-hydroxyl group of the phenyl ring with the oxazoline nitrogen. Oxidized pre-acinetobactin forms a stable H-bond between the hydroxyl group of the hydroxamic acid and the oxazole nitrogen.

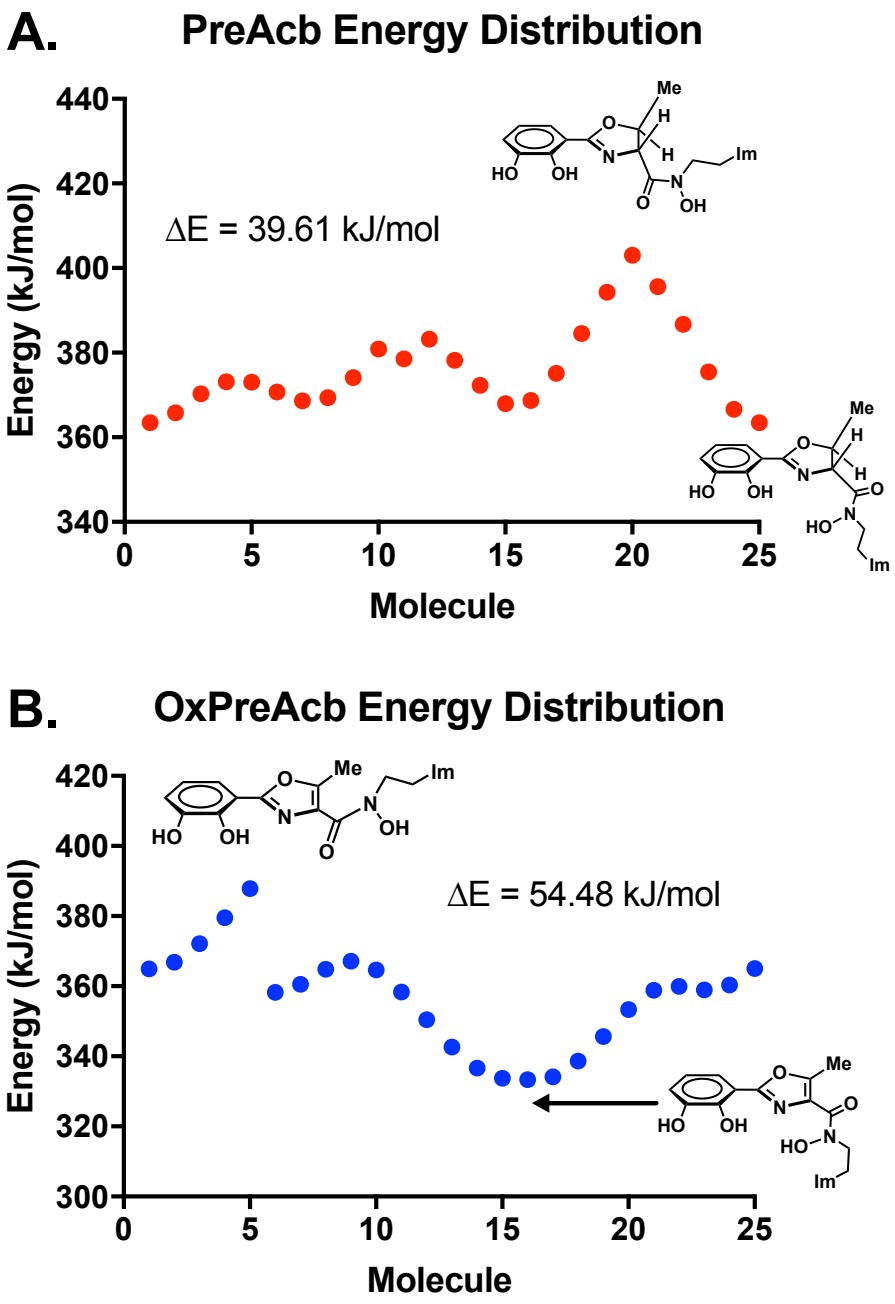

Supplementary Figure 8. Oxidation of pre-acinetobactin oxazoline to the corresponding oxazole restricts rotation about the heterocycle-carbonyl bond through the introduction of $A_{1,3}$ strain. (A.) Energy coordinate diagram for rotation around the oxazoline-carbonyl bond in pre-acinetobactin **1**. (B.) Energy coordinate diagram for rotation around the oxazole-carbonyl bond in oxidized pre-acinetobactin **3**.

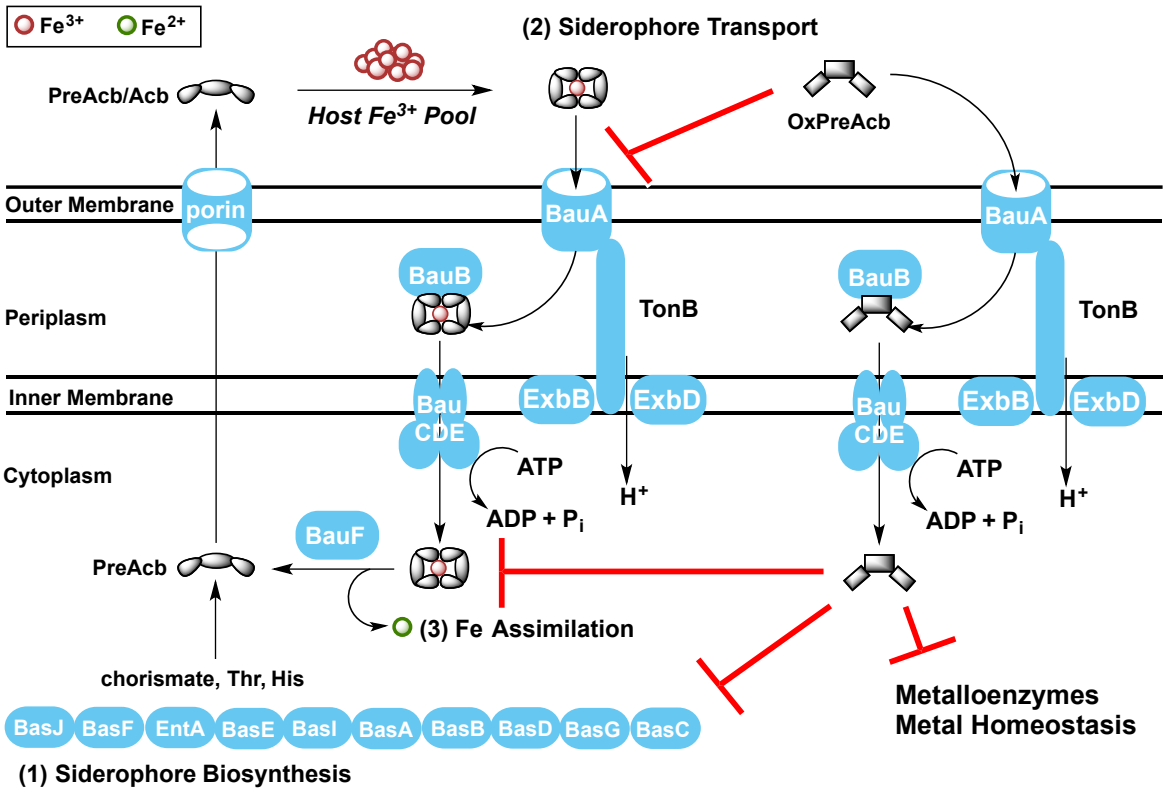

Supplementary Figure 9. Hypothetical model for the mechanism of action of OxPreAcb growth inhibition of *A. baumannii*. Biosynthesis of PreAcb takes place in the cytoplasm. Efflux of PreAcb to the extracellular space provides a mixture of PreAcb and Acb after isomerization spontaneously occurs. PreAcb and Acb form stable complexes $(PreAcb)_2Fe(III)$ and $(Acb)_2Fe(III)$, respectively, that are transported to the periplasmic space by the outer membrane receptor BauA with assistance of the ExbB/ExbD/TonB complex. The periplasmic binding protein BauB shuttles $(PreAcb)_2Fe(III)$ and $(Acb)_2Fe(III)$ to the ABC-transporter BauCDE for transport to the cytoplasm. The flavin reductase BauF is predicted to reduce Fe(III) to Fe(II) and provide PreAcb/Acb for the next siderophore cycle. OxPreAcb is competitive with Acb and inhibits the growth of *A. baumannii*. The mechanism of competition with Acb and growth inhibition is unknown. Competition for transport could take place at the level of BauA on the outside of the cell or BauB on the inside of the cell. Raymond proposed a shuttle mechanism for siderophore transport in Gram-negative bacteria that argues for the involvement of both an iron-bound siderophore and an iron-free siderophore that undergoe metal swapping.[3] The iron-free OxPreAcb might interfere with this siderophore shuttle process, but more fundamental studies of this membrane transport paradigm are required to test this hypothesis. Additionally, OxPreAcb might inhibit siderophore biosynthesis or iron assimilation processes by a competitive mechanism resulting from the structural similarity of OxPreAcb to PreAcb and Acb. Lastly, OxPreAcb was shown to strongly chelate iron(III) so a general mechanism of metalloenzyme inhibition or disruprtion of metal homeostasis might be at play. This type of more general mechanism might account for the growth inhibitory activity of OxPreAcb against non-Acb producing bacteria like *E. coli*.[4]

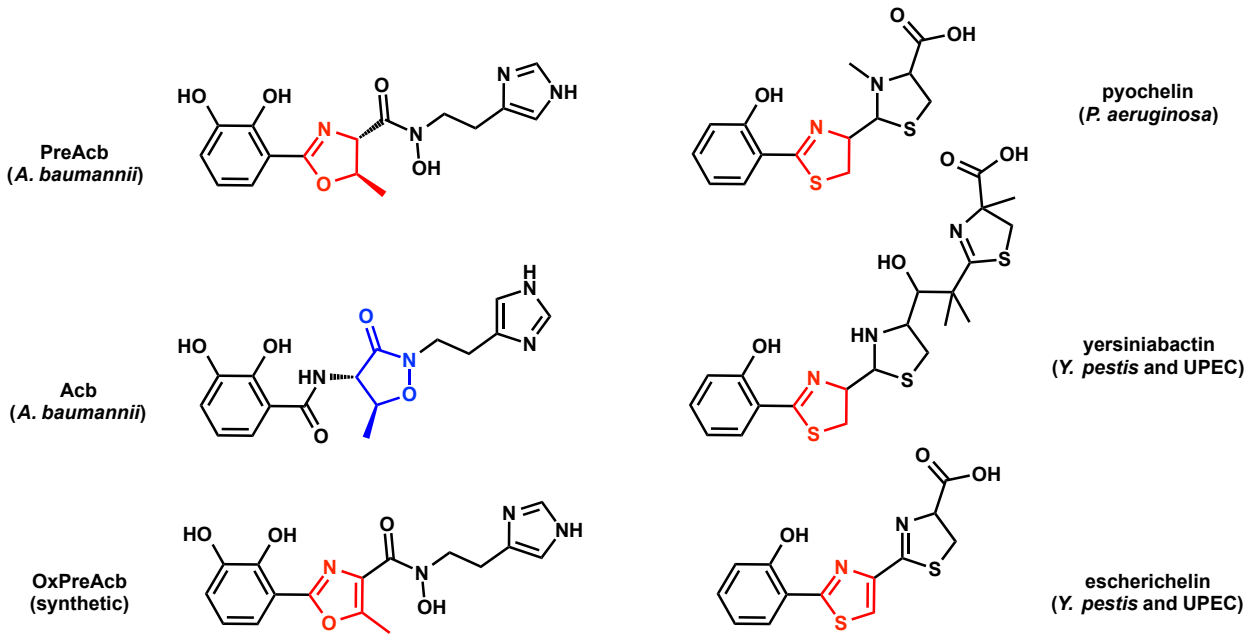

Supplementary Figure 10. Structures of pre-acinetobactin (PreAcb), acinetobactin (Acb), OxPreAcb, pyochelin, yersiniabactin, and escherichelin. OxPreAcb and escherichelin both contain rigid aromatic heterocycles and inhibit the growth of pathogenic bacteria producing structurally similar siderophores with non-aromatic heterocycles.

III. Compound Characterization Data

Benzyl 2-(2,3-dihydroxyphenyl)-5-methyloxazole-4-carboxylate (8)

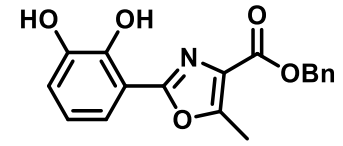

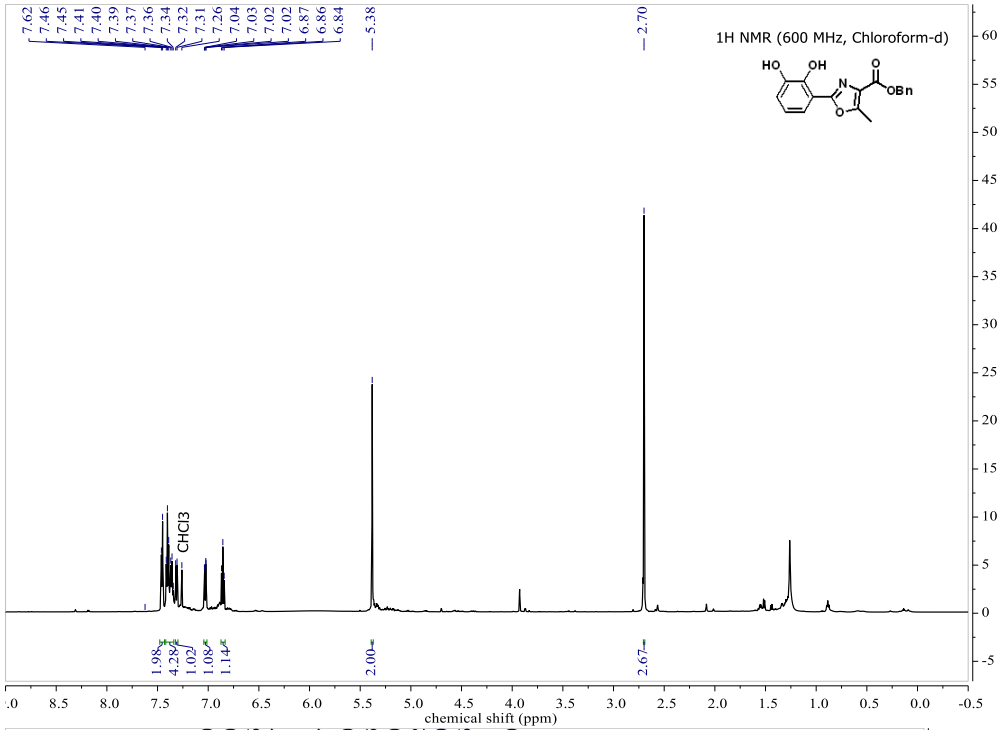

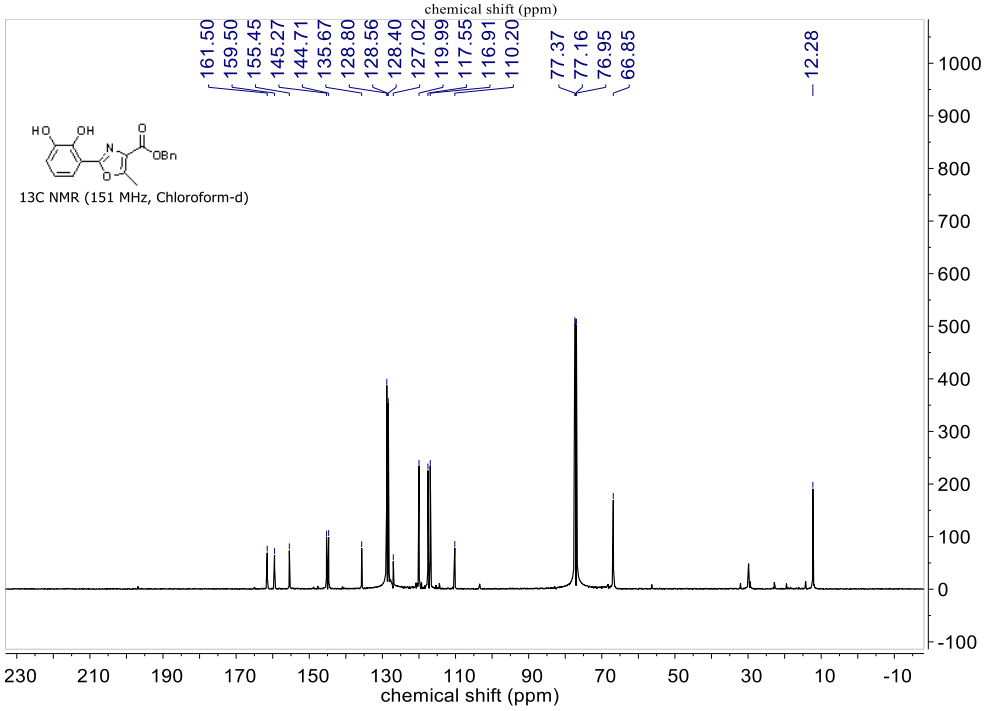

2-(2,3-dihydroxyphenyl)-5-methyloxazole-4-carboxylic acid (9)

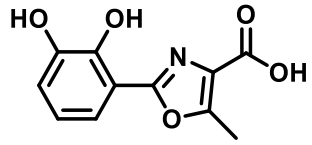

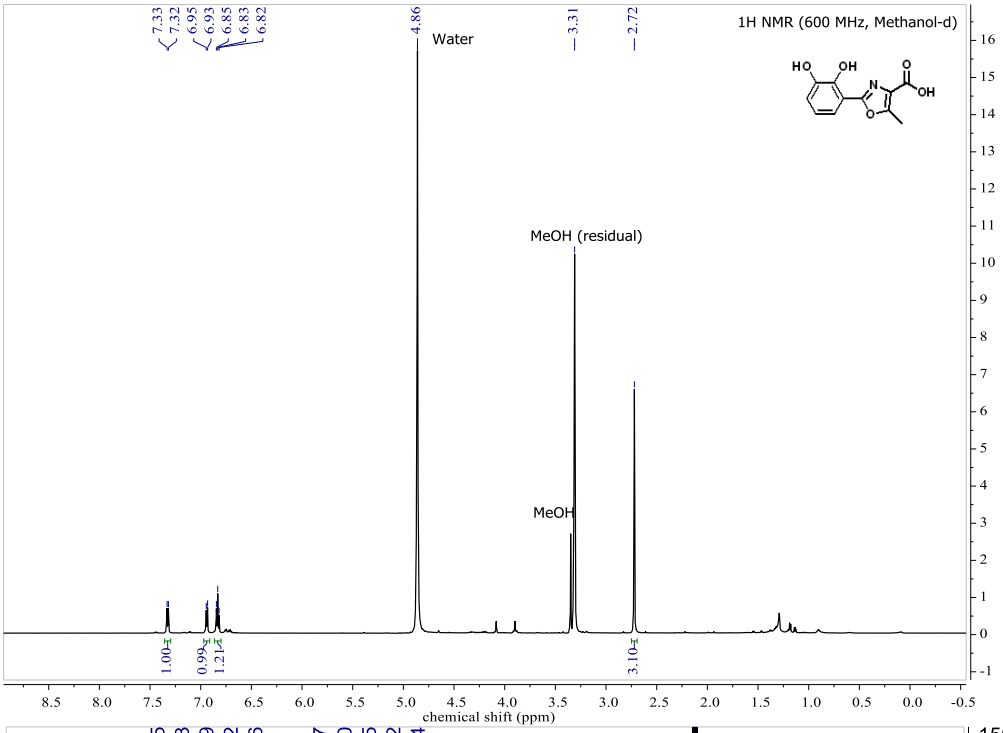

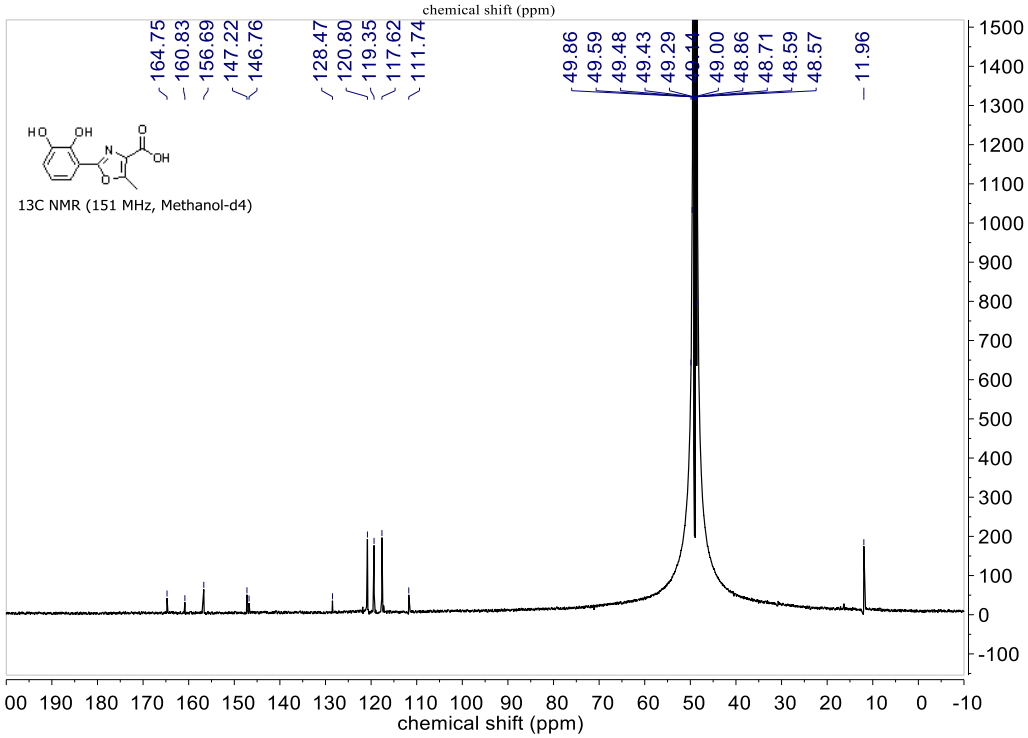

N-(2-(1H-imidazol-4-yl)ethyl)-N-(benzyloxy)-2-(2,3-dihydroxyphenyl)-5-methyloxazole-4-carboxamide (11)

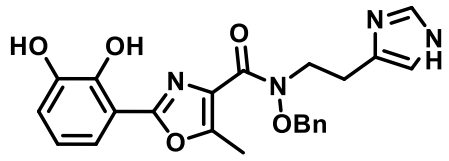

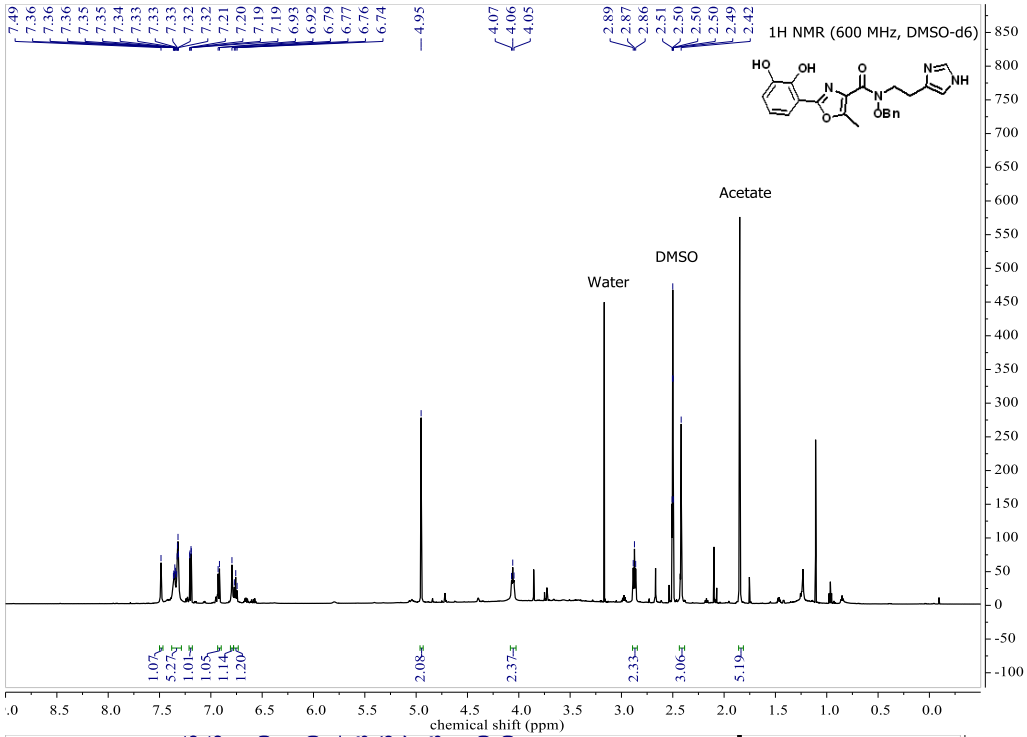

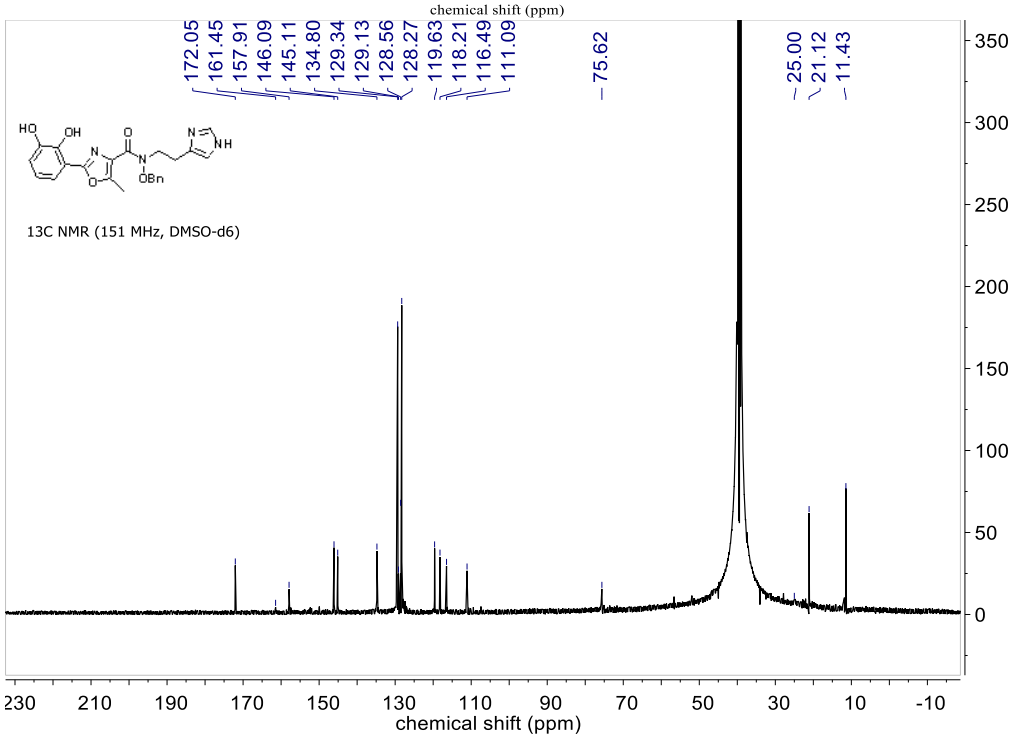

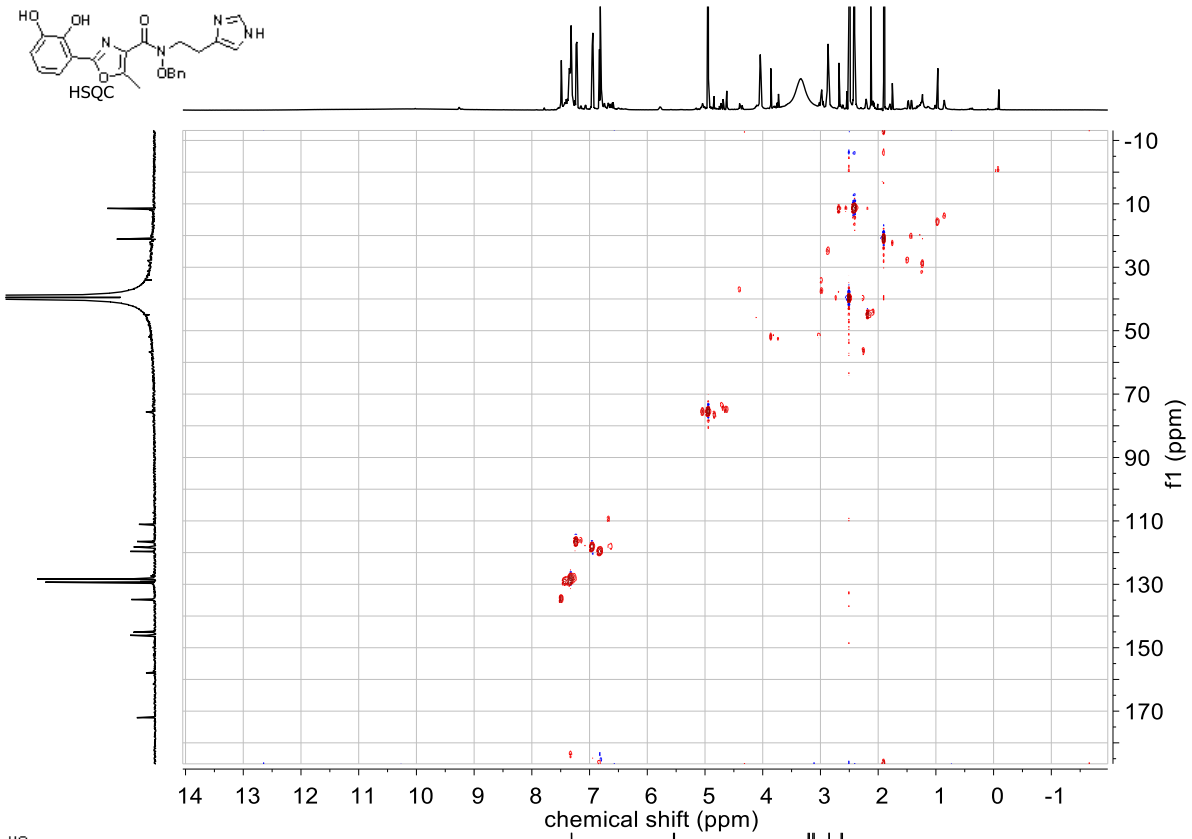
HO
OH
N
O
N
NH
O
N
OBn
HSQC
-10
10
30
50
70
90
110
130
150
170
f1 (ppm)
14 13 12 11 10 9 8 7 6 5 4 3 2 1 0 -1
chemical shift (ppm)

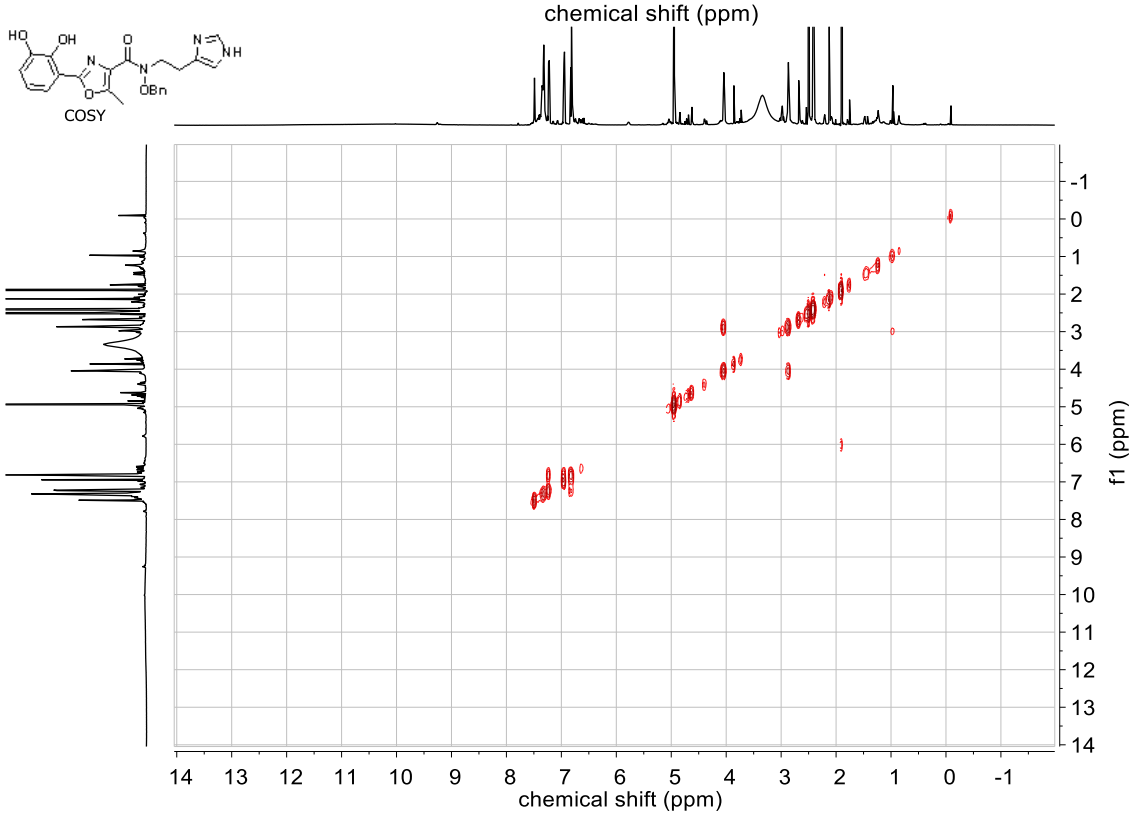
HO
OH
N
O
N
NH
O
N
OBn
COSY
-1
0
1
2
3
4
5
6
7
8
9
10
11
12
13
14
f1 (ppm)
14 13 12 11 10 9 8 7 6 5 4 3 2 1 0 -1
chemical shift (ppm)

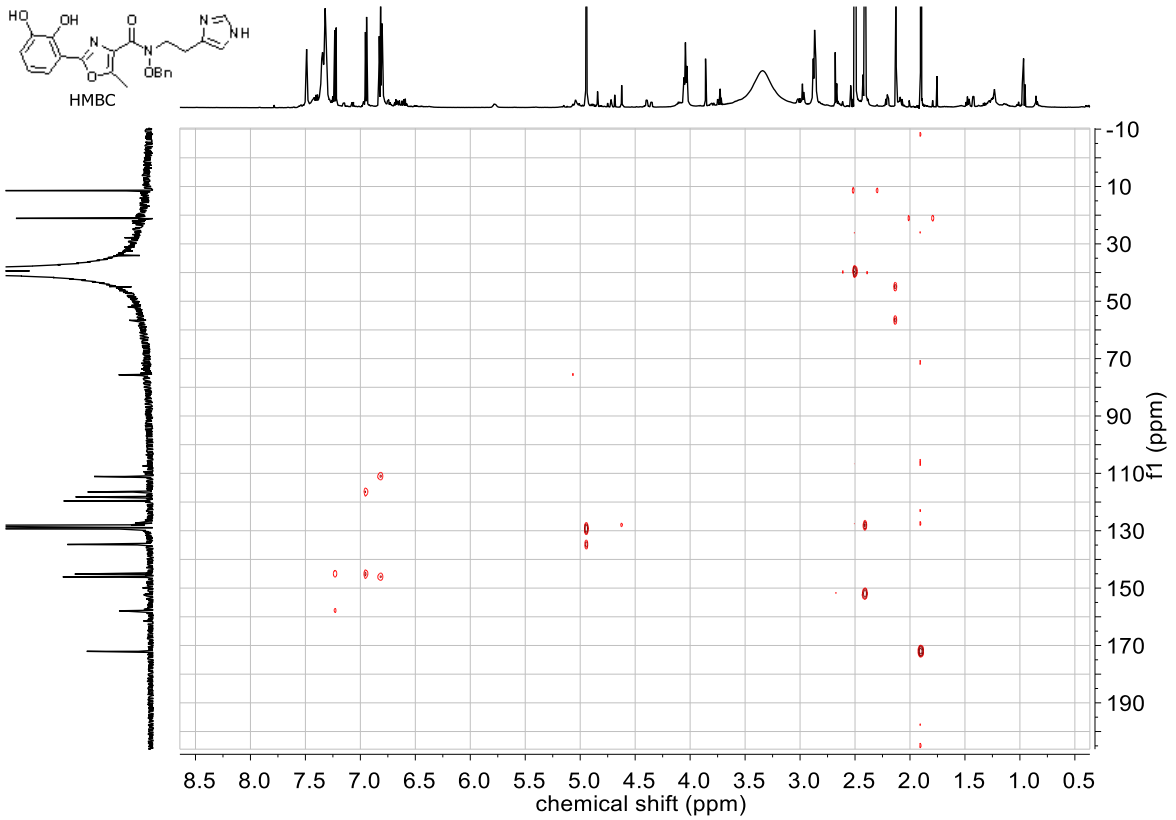
HMBC
f1 (ppm)
chemical shift (ppm)

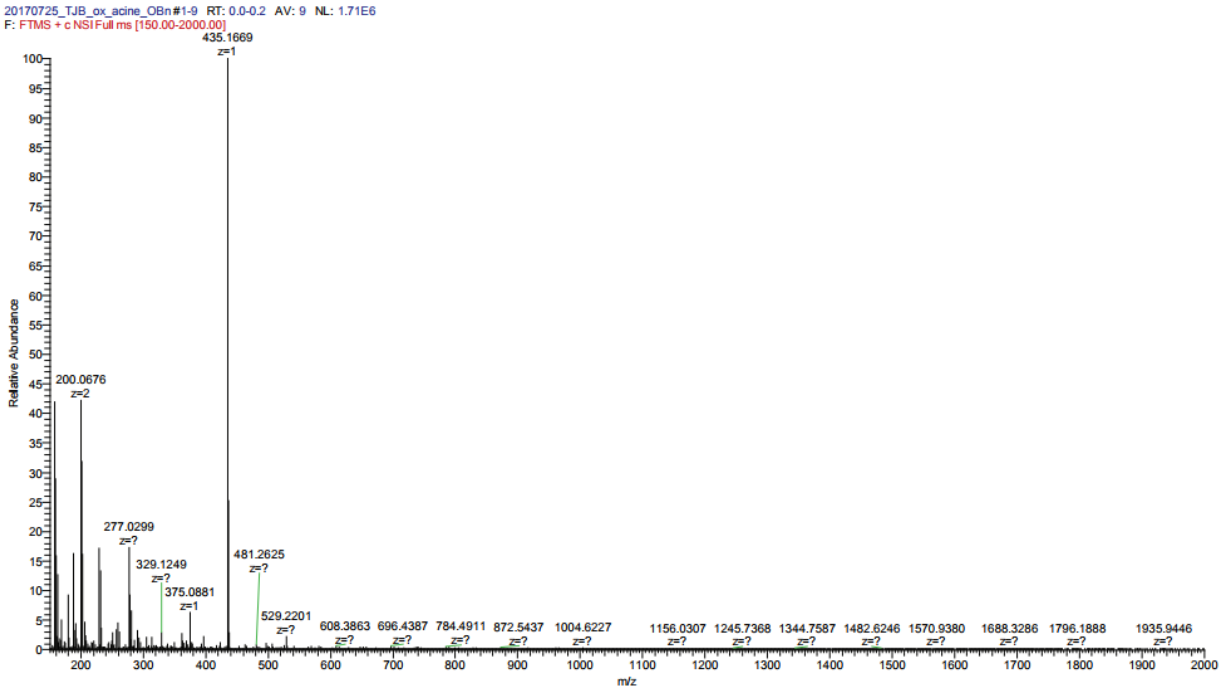
20170725_TJB_ox_acine_OBn#1-9 RT: 0.0-0.2 AV: 9 NL: 1.71E6
F: FTMS + c NSI Full ms [150.00-2000.00]
Relative Abundance
m/z

N-(2-(1H-imidazol-4-yl)ethyl)-2-(2,3-dihydroxyphenyl)-N-hydroxy-5-methyloxazole-4-carboxamide (3)

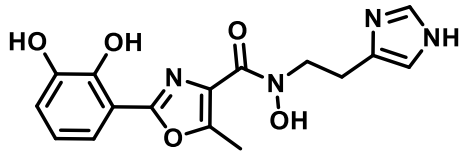

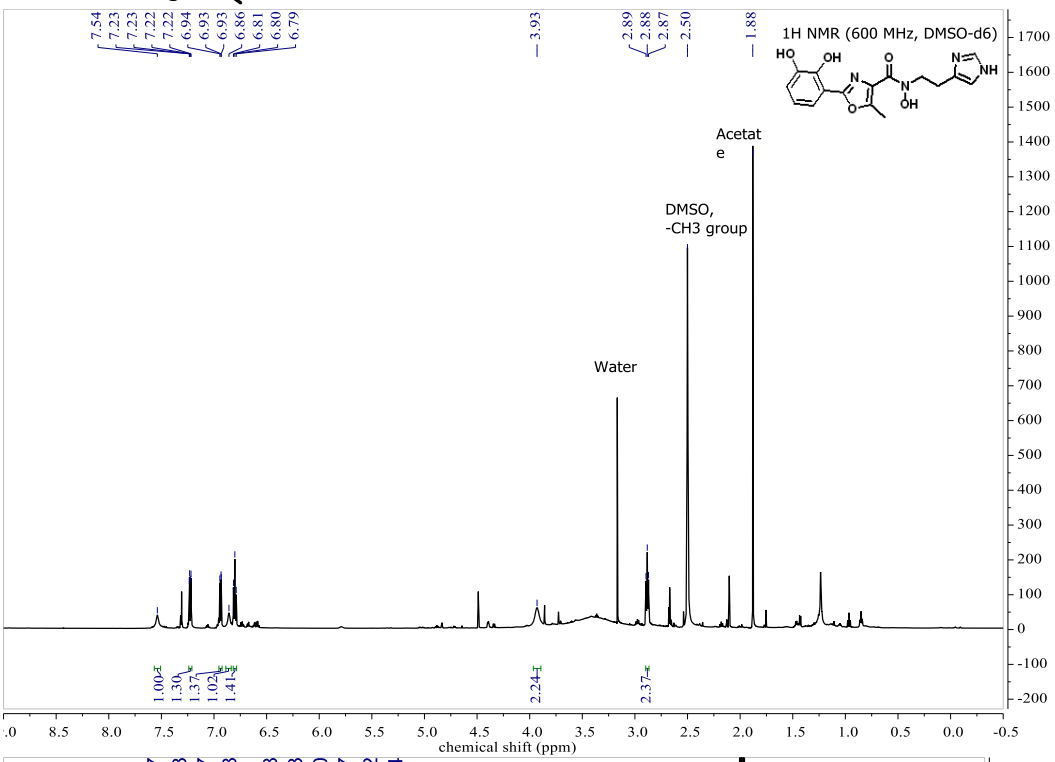

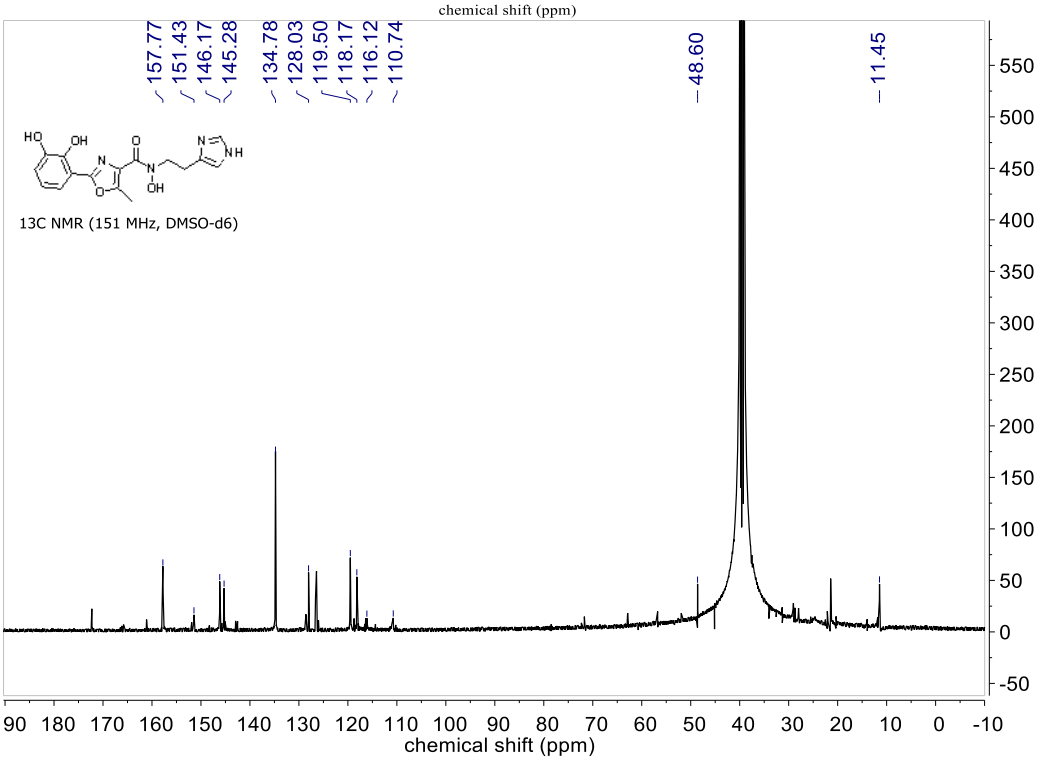

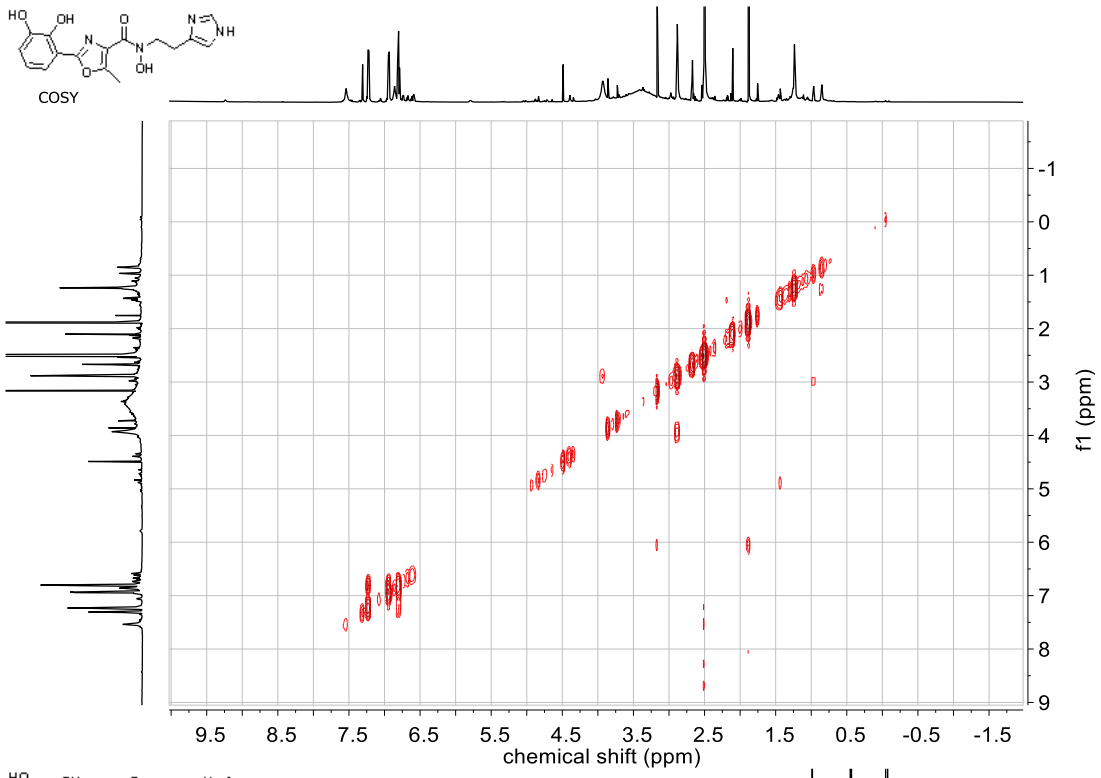
COSY
f1 (ppm)
chemical shift (ppm)

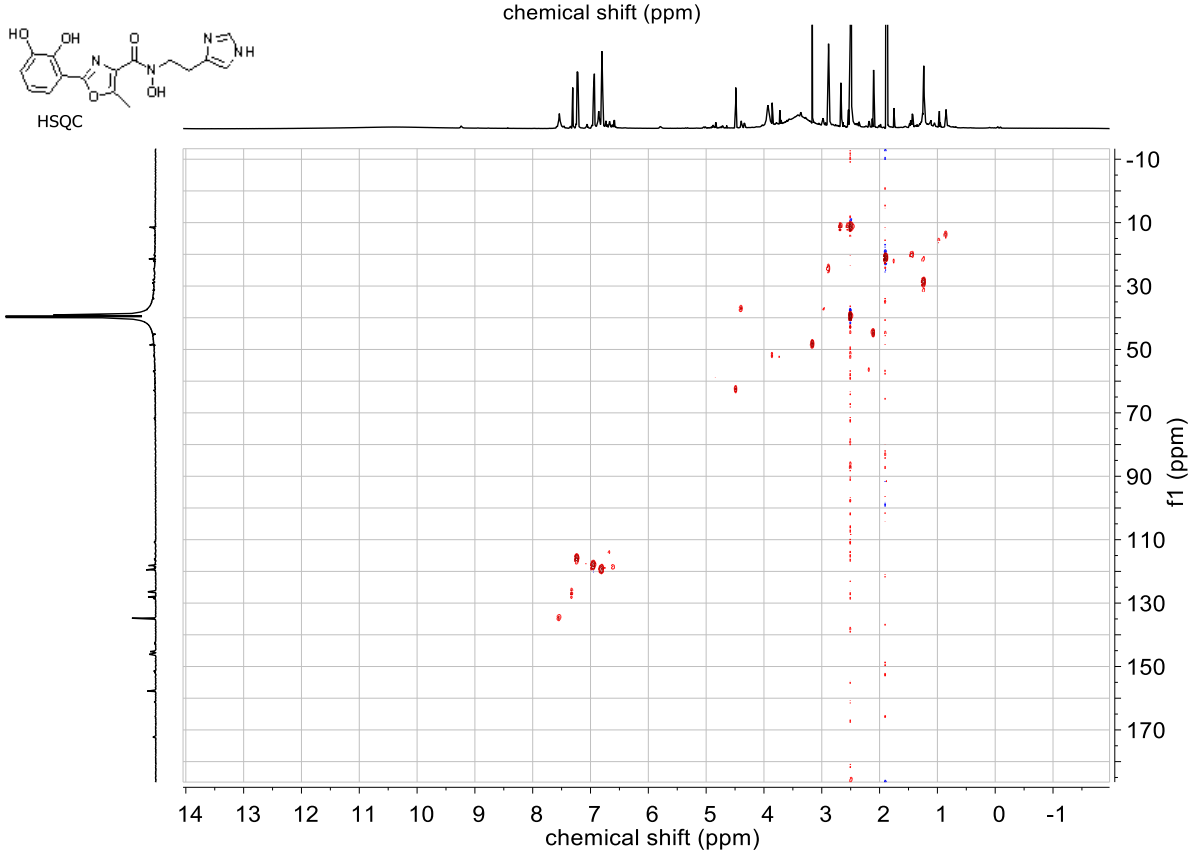
HSQC
f1 (ppm)
chemical shift (ppm)

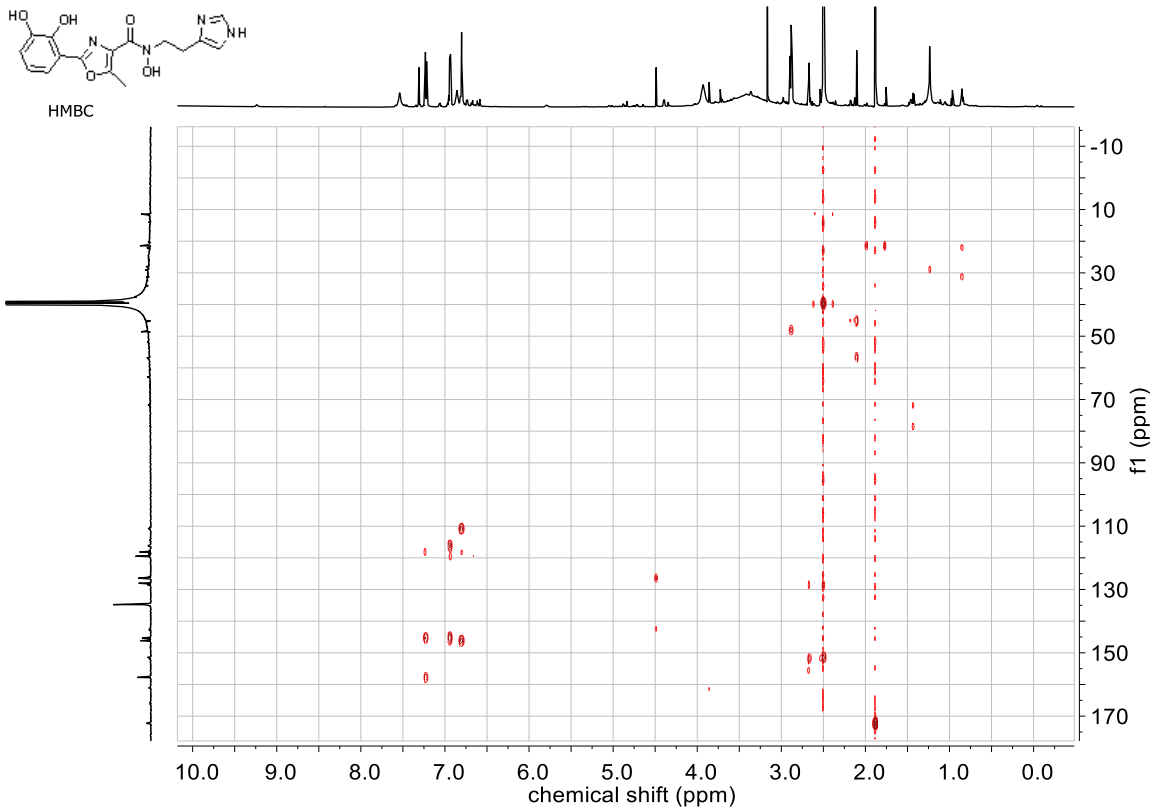

HRMS – OxPreA (3)

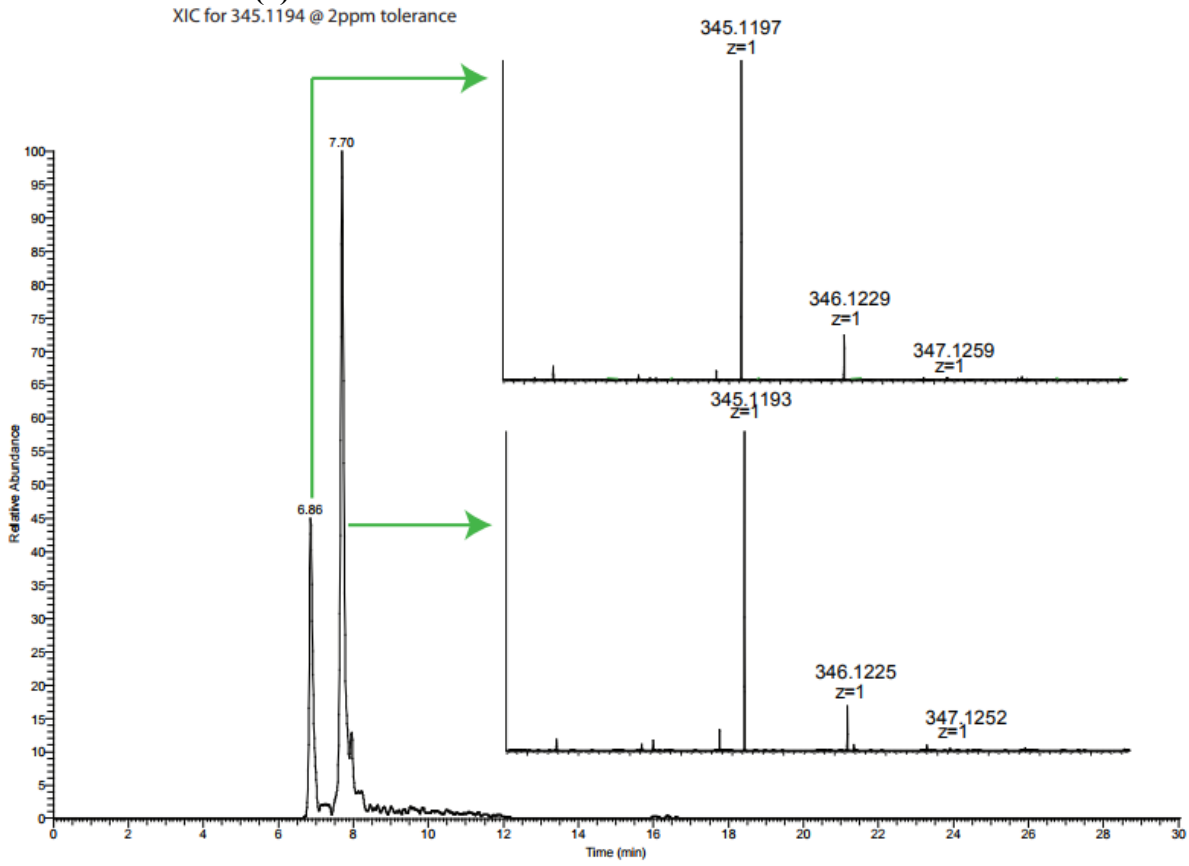

Supplementary Table 1. 2D NMR characterization data of oxidized pre-acinetobactin (**3**) in DMSO-d6.

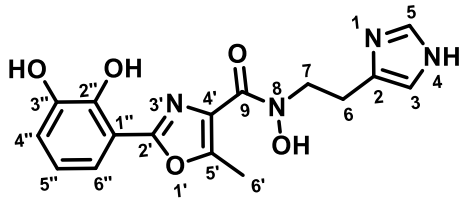

Oxidized Pre-Acinetobactin (**3**)

Atom	^{13}C (ppm)	^{1}H (ppm), Multiplets in Hz	COSY 1H-1H 3 bond	HMBC 1H-13C 2-3 bond	HSQC
2					
3		6.86 (s, 1H)	-	-	-
5	134.8	7.54 (s, 1H)	-	-	5
6	24.9	2.88 (t, 2H)	7	7	6
7	48.1	3.93 (s(br), 2H)	6	-	-
9			-	-	-
2’	157.8		-	-	-
4’	128.0		-	-	-
5’	151.5		-	-	-
6’	11.5	2.50 (s, 3H)	-	5’	6’
1’’	110.7		-	-	-
2’’	145.3		-	4’’,6’’	-
3’’	146.2		-	5’’	-
4’’	118.2	6.92-6.95 (m, 1H)	5’’	2’’,5’’	4’’
5’’	119.6	6.80 (t, 1H)	6’’	3’’,4’’	5’’
6’’	116.1	7.23 (dd, 1H)	5’’	2’,2’’,4’’	6’’

OxPreAcb (TFA salt)

OxPreAcb (**3**) was re-purified by preparatory HPLC upon reviewer request. Prep HPLC was performed with a mobile phase of 0.1% trifluoroacetic acid in (A) water and (B) acetonitrile (gradient of 0% B to 95% B in 17 min, 95% B to 100% B in 2 min, hold 100% B for 8 min). See 1H NMR and LC-MS below. This batch of OxPreA was higher purity and reproduced the iron-dependent growth inhibitory effects on *A. baumannii* (**Supplementary Fig. 1**).

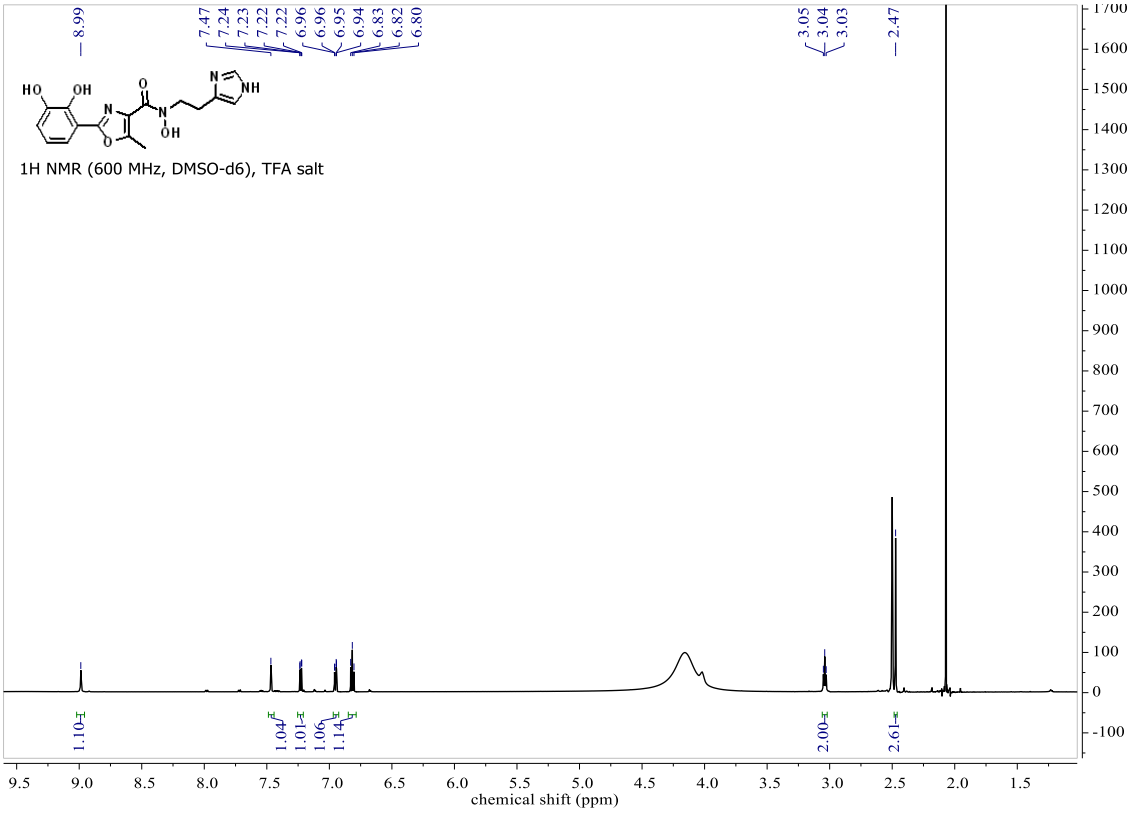

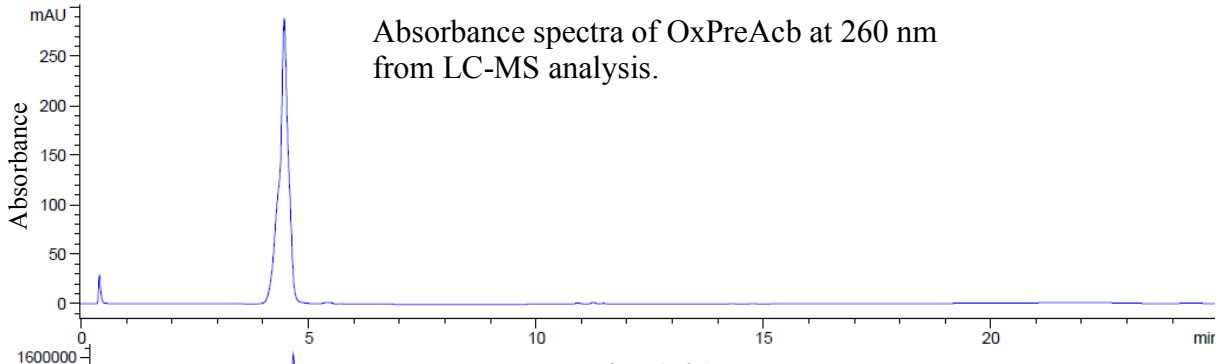

Absorbance spectra of OxPreAcb at 260 nm from LC-MS analysis.

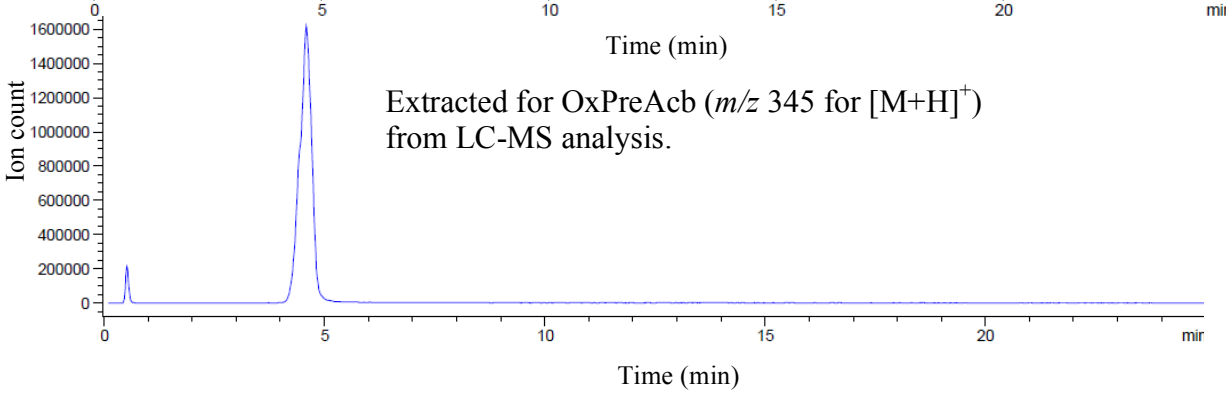

Extracted for OxPreAcb (*m/z* 345 for $[M+H]^+$) from LC-MS analysis.

IV. Acknowledgements

The authors would like to thank Drs. Jeff Kao and Manmilan Singh (WUSTL Chemistry) for help with the acquisition of 2D NMR data and Dr. Bradley Evans (Danforth Plant Science Center, St. Louis, MO; NSF DBI-0521250) for help with the acquisition and processing of HRMS data. Research was supported by NSF CAREER Award 1654611 to TAW.

V. References

(1) Shapiro J.A.; Wencewicz T.A. *ACS Infect Dis*. **2016**, *2*, 157-168

(2) Graham T.H. *Org. Lett.* **2010**, *12*, 3614-3617

(3) Stintzi, A.; Barnes, C.; Xu, J.; Raymond, K. N. *Proc. Natl. Acad. Sci. U.S.A*. **2000**, *97*, 10691-10696.

(4) Chan, A. N.; Shiver, L. S.; Wever, W. J.; Razvi, S. Z. A.; Traxler, M. F.; Li, B. *Proc. Natl. Acad. Sci. U.S.A*. **2017**, *10*, 2717-2722.